IEEE Access
Multidisciplinary ⋮ Rapid Review ⋮ Open Access Journal

Received December 17, 2020, accepted December 24, 2020, date of publication January 8, 2021, date of current version January 13, 2021.

Digital Object Identifier 10.1109/ACCESS.2021.3049644

A Joint Framework for Seismic Signal Denoising Using Total Generalized Variation and Shearlet Transform

XIANNAN WANG[1], JIAN ZHANG[1], AND HAO CHENG[2]
[1]School of Equipment Engineering, Shenyang Ligong University, Shenyang 110159, China
[2]Key Laboratory of Ministry of Education on Safe Mining of Deep Metal Mines, Northeastern University, Shenyang 110819, China

Corresponding author: Jian Zhang (zbgc2003@163.com)

This work was supported in part by the National Natural Science Foundation of China under Grant 41804103, and in part by the Fund for Equipment Pre-research of China under Grant 61406190105.

ABSTRACT Seismic exploration is a remote-sensing tool applied in a great many projects for engineering and resource-exploration purposes. Random noise suppression is one of the key steps in seismic-signal processing, especially those with important details and features. The threshold-shrinkage method based on Shearlet transform has been effectively applied in seismic-signal denoising. However, the method usually introduces the boundary effect, which influences the imaging quality. The denoising method of total generalized variation (TGV) is easy to produce 'oil painting' effect, but it can effectively suppress the boundary effect. This paper proposes a denoising method based on Shearlet threshold-shrinkage and TGV for making full use of their characteristics, which can recover both edges and fine details much better than the existing regularization methods. First, we use the Shearlet threshold-shrinkage result as the input of TGV to obtain the primary denoising result and the residual profile. Second, we use the interactive iteration of Shearlet threshold-shrinkage and TGV to extract the signals efficiently from the residual profile and perform the effective signals stack continuously. During the processing, the adaptive-weight factor is combined for estimating the optimal denoising result. Last, the final estimated denoising result is obtained when the stopping criterion is met or the maximum number of iterations is reached. The synthetic and field results show that the proposed method can effectively suppress random noise. In addition, it can also remove the boundary effect and 'oil painting' effect, which further improves the signal-to-noise ratio (SNR).

INDEX TERMS Noise suppression, Shearlet transform, TGV, adaptive-weight factor, SNR.

I. INTRODUCTION

Seismic exploration, as one of the geophysical techniques, is a significant remote-sensing tool and applied in a great many projects for engineering and resource-exploration purposes [1]–[3]. In seismic-data acquisition, it is usually corrupted by various noise, such as the acquisition environment and acquisition devices. Seismic signals contain a large amount of random noise, which reduces SNR and recognition accuracy. This is not conducive to subsequent processing and final profile interpretation. Therefore, random noise suppression [4]–[8] is one of the key steps in seismic-data processing [9]–[10].

The associate editor coordinating the review of this manuscript and approving it for publication was Wenming Cao.

Sparse-transform denoising is one of the main methods for random noise suppression. According to the difference of the corresponding coefficients between the effective signals and random noise in the transform domain, the appropriate threshold calculation method can be selected to separate the effective signals and random noise for the denoising purpose. The sparse-transform denoising methods usually include Wavelet transform [11], Contourlet transform [12], Curvelet transform [13], etc. They play important roles in the sparse representation and image processing of two-dimensional and high-dimensional signals. But their physical meanings are not clear enough. The size of the coefficient matrix corresponding to the special scale and angle in the transform domain is different from the original data.

Shearlet transform [14]–[18], as a new sparse-transform method, has the multi-scale and multi-direction

characteristics. That can optimally describe the local characteristics of the signals. Fewer coefficients are used for approximating curves. Compared with other multi-scale analysis methods, Shearlet transform has a simpler mathematical structure, which is more exquisite for characterizing the scale and direction of the signals. That is suitable for processing seismic data which contains texture, contour, and boundary information. Liu *et al.* [19] introduced 2D-Shearlet transform to suppress random noise of seismic data, and prove the denoising effectiveness of Shearlet transform. On this basis, Cheng *et al.* [20] proposed an adaptive threshold during the Shearlet denoising for improving SNR while retaining the effective signals to the maximum extent simultaneously. He also extended the adaptive-threshold denoising to 3D-Shearlet transform [21]. This threshold-shrinkage processing will introduce the boundary effect. That may cause the false stratums, which has a negative impact on the structure interpretation of seismic signals.

The total variation (TV) [22] method can preserve the boundary information while suppressing random noise. However, it only considered the first derivative, which easily causes 'oil painting' effect. Bredies *et al.* [23] proposed the total generalization variation (TGV) method, which fully considered the influence of higher order derivatives. On the basis of the balance between the calculating time and the imaging quality, they extended to the second derivative, which suppresses the 'oil painting' effect to a certain extent. That makes the quality of the denoising results are improved, but sometimes it is still not ideal.

In order to make up for the drawbacks of sparse-transform and TGV denoising methods and make full use of the advantages of both, Sylvain and Jacques [24] combined the wavelet de-noising and TV regularization methods to realize the advantageous complementarities. Hu *et al.* [25] introduced TV model to Shearlet de-noising for suppressing random noise and preserving the edge information effectively. Tang and Ma [26] extended Curvelet de-noising and TV methods to 3D seismic data by the same way. In order to suppress the boundary effect caused by threshold de-noising in the Shearlet domain, Kong and Peng [27] combined with TGV regularization for random noise suppression.

TGV can preserve the boundaries but suffer from 'oil-painting' artifacts. Shearlet-based denoising method can suppress random noise well, but often suffer from unwanted artifacts, e.g., the boundary effect. To overcome these drawbacks, a joint framework using TGV and Shearlet is proposed for seismic random noise suppression. The results of Shearlet threshold shrinkage is used as input to the TGV method, which can be used to suppress the boundary effect. By this way, the 'oil painting' effect caused by TGV can be reduced at the same time. During the iterations, the weight factors of the regularized item are adaptively changed. The best denoising results can be estimated by extracting the effective information from the residual profile. By this way, the imaging quality can be improved well by taking advantage of the fact that two techniques benefit from each other. This approach performs a nearly artifact-free signals denoising. The synthetic and field data are used for testing to verify the effectiveness and accuracy of the proposed method, respectively.

II. SHEARLET DE-NOISING METHOD

A. SHEARLET TRANSFORM

The affine system formed by Shearlet is composed of expansion and translation parts. The expansion part contains an anisotropic parabolic scale matrix and a shear matrix. In order to define the Shearlet system, the parabolic scale matrix and the shear matrix are defined as A_c, $c \in \mathbb{R}^+$ and S_b, $b \in \mathbb{R}$, respectively, expressed as follows

$$A_c = \begin{pmatrix} c & 0 \\ 0 & \sqrt{c} \end{pmatrix} S_b = \begin{pmatrix} 1 & -b \\ 0 & 1 \end{pmatrix} \tag{1}$$

Then, the Shearlet system can be expressed as

$$\left\{ \psi_{g,h,m}(x) := 2^{-\frac{3}{2}g} \psi(S_{-h} A_{4-g} x - m) : g, h \in \mathbb{Z}, m \in \mathbb{Z}^2 \right\} \tag{2}$$

In the formula, g is the scale parameter, h is the angle parameter and m is the position parameter. By choosing

$$\hat{\psi}(\xi_1, \xi_2) = \hat{\psi}_1(\xi_1) \hat{\psi}_2(\xi_2 / \xi_1) \tag{3}$$

Here, $\psi_1 \in L^2(\mathbb{R})$ is a discrete wavelet, $\sum_{g \in \mathbb{Z}} \left| \hat{\psi}_1(4^g \omega) \right|^2 = 1$, $\omega \in \mathbb{R}$, $\hat{\psi}_1 \subset [-1, -1/4] \cup [1/4, 1]$, $\psi_2 \in L^2(\mathbb{R})$ is a Bump function. $\hat{\psi}_2 \in C^\infty(\mathbb{R})$, $\hat{\psi}_2 \subset [-1, 1]$, $\sum_{h \in \mathbb{Z}} \left| \hat{\psi}_2(h + \omega) \right|^2 = 1$. $\xi_1, \xi_2 \in \mathbb{R}$. The Shearlet transform of an arbitrary function f can be expressed as

$$SH_\psi f(g, h, m) = \langle f, \psi_{g,h,m} \rangle \tag{4}$$

B. CHARACTERISTICS OF SHEARLET TRANSFORM

Figures 1 and 2 show the shapes of the Shearlet-basis functions in the frequency and time domains respectively. Figure 1 shows the Shearlet-basis functions in different directions at the third scale. Figure 2 shows the Shearlet-basis functions at the second, third and fourth scales in the 45-degree direction. Figures 1 and 2 show the multi-scale and multi-directional characteristics of Shearlet transform.

The multi-scale and multi-directional characteristics of Shearlet transform can effectively divide the seismic signals, as shown in Figure 3. Figure 3a is the synthetic seismic signals. Figure 3b-e are part of the synthetic-signal coefficients in the Shearlet domain, which shows the ability of dividing the seismic signals.

We also compare Shearlet transform with Curvelet transform and Contourlet transform at the aspect of the sparsity. The seismic signals of Figure 3a is decomposed with different transform methods. The coefficients are arranged from large to small, and different percentages of coefficients are retained for reconstruction. The error between the reconstructed and original signals is calculated. Figure 4 shows a comparison of the reconstruction errors of the three transforms, with the maximum percentage of coefficients retained ranging

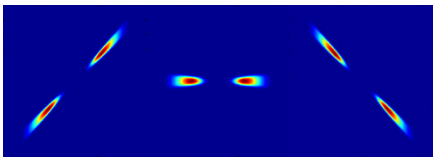

(a) Frequency domain

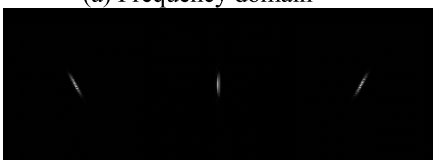

(b) Time domain

FIGURE 1. Different direction in third scale of Shearlet-basis function.

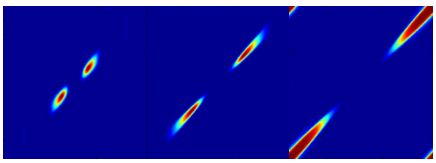

(a) Frequency domain

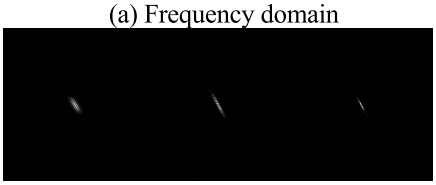

(b) Time domain

FIGURE 2. Different scales in 45 degree direction of Shearlet-basis function.

from 0.5% to 30%. When the maximum coefficient of 4% is retained, the reconstruction error of Shearlet transform is almost zero. While Curvelet transform and Contourlet transform retain the maximum coefficient of 10%, the reconstruction error is nearly zero. That indicates Shearlet transform has the better sparsity.

C. SHEARLET THRESHOLD SHRINK DE-NOISING

The noise signals u can be expressed as the sum of effective signals u_0 and random noise n, which can be defined by the following model

$$u = u_0 + n \tag{5}$$

In the Shearlet domain, the effective signals can be separated from random noise by setting appropriate thresholds. The hard threshold function T used can be defined as

$$T(s) = \begin{cases} s, & |s| \geq C \cdot \lambda \cdot \sigma \\ 0, & |s| < C \cdot \lambda \cdot \sigma \end{cases} \tag{6}$$

In the formula, s represents the Shearlet coefficient. C is a constant. λ is the root mean square of the Shearlet coefficient at a certain scale and angle, which changes with the change of scale and angle. σ is the standard deviation of noise. Then, the inverse Shearlet transform is performed on the retained coefficients to obtain the denoising result.

III. TGV DE-NOISING METHOD

Total variation (TV) is widely used in signal processing because of its good characteristics. TV minimization means that the L1 norm of the first-order derivative of the input data is the smallest. However, TV minimization uses the first-order derivative, which will cause the 'oil painting' effect. Therefore, TGV method is proposed. The purpose of using TGV regularization constraints is to preserve the boundaries and suppress the introduced 'oil painting' effect.

For $u \in L^1_{loc}(\boldsymbol{\Omega})$, the t-th order TGV can be defined as

$$TGV^t_\alpha(u) = \sup \left\{ \begin{array}{l} \int_{\boldsymbol{\Omega}} u \cdot \mathrm{div}^t w dx | w \in C^t_c[\Omega, Sym^t(\boldsymbol{R}^d)], \\ \left\| \mathrm{div}^l w \right\|_\infty \leq \alpha_l, l = 0, \cdots, t-1 \end{array} \right\} \tag{7}$$

In the formula, $\alpha = (\alpha_0, \cdots \alpha_{t-1})$ is a weight factor which is fixed to be positive. $t \geq 1$ represents a derivative order. $C^{\mathrm{t}}_c[\boldsymbol{\Omega}, Sym^t(\boldsymbol{R}^d)]$ is a tightly supported symmetric vector space. In fact, TVG method uses a balance between first-order and the t-order derivative. When $t = 1$ and $\alpha = 1$, TVG is equivalent to TV. TVG usually uses 2-nd order derivative for data processing, which is defined as follows

$$TGV^2_\alpha(u) = \sup \left\{ \begin{array}{l} \int_\Omega u \cdot \mathrm{div}^2 w dx | w \in C^2_c(\Omega, R^{d \times d})], \\ \|w\|_\infty \leq \alpha_1, \|\mathrm{div} w\|_\infty \leq \alpha_2 \end{array} \right\} \tag{8}$$

In the formula, div represents the scatter of the sampled data. The first and second order derivative can be defined as

$$(\mathrm{div} w)_i = \sum_{j=1}^{d} \frac{\partial w_{ij}}{\partial x_j} \mathrm{div}^2 w = \sum_{j=1}^{d} \frac{\partial^2 w_{ij}}{\partial x_j^2} + 2 \sum_{i<j} \frac{\partial^2 w_{ij}}{\partial x_i \partial x_j} \tag{9}$$

TGV can be rewritten as a combination of p and its derivatives $\zeta(p)$, defined as follows

$$\begin{aligned} TGV^2_\alpha(u) &= \alpha_0 \|\nabla u - p\|_1 + \alpha_1 \|\zeta(p)\|_1 \\ \zeta(p) &= \begin{bmatrix} \partial_x p_1 & \frac{1}{2}(\partial_x p_2 + \partial_y p_1) \\ \frac{1}{2}(\partial_x p_2 + \partial_y p_1) & \partial_y p_2 \end{bmatrix} \end{aligned} \tag{10}$$

Which p is the estimated first-order derivative. α_0 and α_1 are weight factors.

IV. JOINT DENOISING METHOD OF SHEARLET AND TGV

The threshold shrinkage method in the Shearlet domain has strong denoising ability. Due to the change of Shearlet coefficients, it usually causes the boundary effect and influences the imaging quality. The TGV denoising method, under the interference of random noise, usually produces the 'oil painting' effect. The 'oil painting' effect can be reduced significantly by using the Shearlet threshold denoising results as the input of TGV. TGV can only be used to remove the boundary effect caused by the Shearlet threshold method. However, TGV has a strong damage to the effective signals. Therefore, the interactive iteration between Shearlet denoising and TGV is needed. That can continuously extract effective signals from the residual profile. In this way, the satisfying results can be obtained.

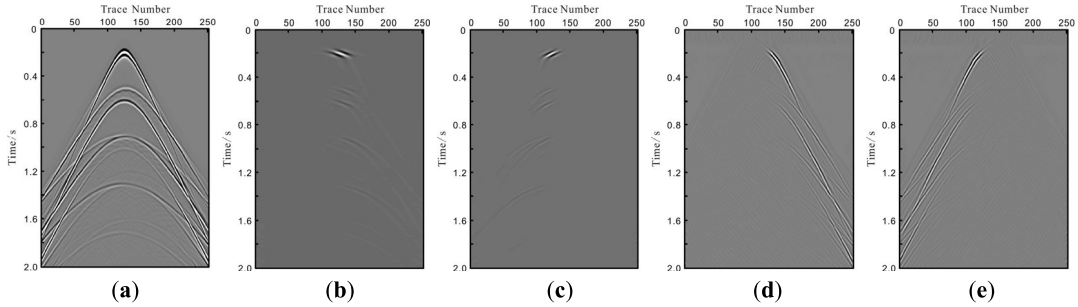

FIGURE 3. (a) Synthetic data. (b)-(e) Part of coefficients of synthetic data in the Shearlet domain.

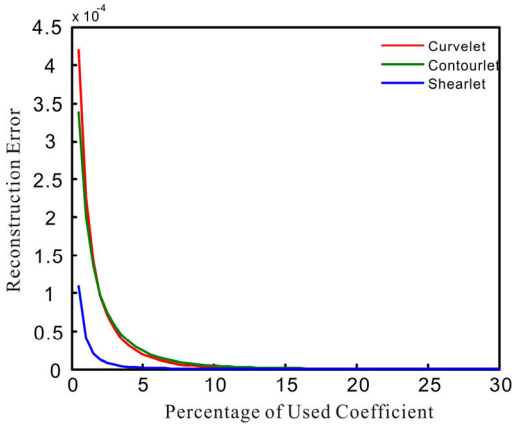

FIGURE 4. Comparison of the reconstruction error.

Here, Q_{SH} represents the result of the Shearlet denoising method. Q_{SH} can be expressed as

$$Q_{\mathrm{SH}}(u) = SH^{-1}(T(SH(u))) \tag{11}$$

In the formula, SH represents the Shearlet forward transform. SH^{-1} represents the inverse Shearlet transform. Substituting Q_{SH} into TGV, it can be expressed as

$$\tilde{u} = Q_{\mathrm{SHTGV}}(\mathrm{u}) = TGV(Q_{\mathrm{SH}}) \tag{12}$$

where $\tilde{u}$ is the estimated de-noising result. Q_{SHTGV} is the denoising result after Shearlet and TGV denoising methods. The calculation model can be expressed as

$$\min_{Q_{\mathrm{SH}},p} \frac{1}{2} \left\| Q_{\mathrm{SH}} - \tilde{u} \right\|_2^2 + \alpha_0 \left\| \nabla Q_{\mathrm{SH}} - p \right\|_1 + \alpha_1 \left\| \zeta(p) \right\|_1 \tag{13}$$

Using the auxiliary variables z1 and z2, the above formula can be rewritten as

$$\begin{aligned} &\min_{Q_{\mathrm{SH}},p} \frac{1}{2} \left\| Q_{\mathrm{SH}} - \tilde{u} \right\|_2^2 + \alpha_0 \left\| z_1 \right\|_1 + \alpha_1 \left\| z_2 \right\|_1 \\ &s.t. z_1 = \nabla Q_{\mathrm{SH}} - p z_2 = \zeta(p) \end{aligned} \tag{14}$$

The above formula is a constrained optimization problem, which can be converted into a non-constrained optimization problem for solving.

$$\begin{aligned} &\min_{Q_{\mathrm{SH}},p} \frac{1}{2} \left\| Q_{\mathrm{SH}} - \tilde{u} \right\|_2^2 + \alpha_0 \left\| z_1 \right\|_1 + \alpha_1 \left\| z_2 \right\|_1 \\ &+ \frac{\mu}{2} \left\| z_1 - \nabla Q_{\mathrm{SH}} + p - \tilde{z}_1 \right\|_2^2 + \frac{\mu}{2} \left\| z_2 - \zeta(p) - \tilde{z}_2 \right\|_2^2 \end{aligned} \tag{15}$$

The parameter μ is a Lagrangian multiplier. The iterative optimization steps according to ADMM can be defined as follows

$$\begin{aligned} z_1^{n+1} &= \arg\min_{z_1} \alpha_0 \left\| z_1 \right\|_1 \\ &\quad + \frac{\mu}{2} \left\| z_1 - \nabla Q_{\mathrm{SH}}^{\mathrm{n}} + p^n - \tilde{z}_1^n \right\|_2^2 \end{aligned} \tag{16}$$

$$\begin{aligned} z_2^{n+1} &= \arg\min_{z2} \alpha_1 \left\| z_2 \right\|_1 \\ &\quad + \frac{\mu}{2} \left\| z_2 - \zeta(p^n) - \tilde{z}_2^n \right\|_2^2 \end{aligned} \tag{17}$$

$$\begin{aligned} (Q_{\mathrm{SH}}^{n+1}, p^{n+1}) &= \min_{u,p} \frac{1}{2} \left\| Q_{\mathrm{SH}} - \tilde{u} \right\|_2^2 \\ &\quad + \frac{\mu}{2} \left\| z_1^{n+1} - \nabla Q_{\mathrm{SH}}^n + p^n - \tilde{z}_1^n \right\|_2^2 \\ &\quad + \frac{\mu}{2} \left\| z_2^{n+1} - \zeta(p^n) - \tilde{z}_2^n \right\|_2^2 \end{aligned} \tag{18}$$

$$\tilde{z}_1^{n+1} = \tilde{z}_1^n + \mu(\nabla Q_{\mathrm{SH}}^{n+1} - p^{n+1} - z_1^{n+1}) \tag{19}$$

$$\tilde{z}_2^{n+1} = \tilde{z}_2^n + \mu(\zeta(p^{n+1}) - z_2^{n+1}) \tag{20}$$

By the calculation above, the output can be obtained

$$\tilde{u} = Q_{\mathrm{SHTGV}}^{\mathrm{k=1}}(u) = Q_{\mathrm{SH}}^{\mathrm{n+1}} \tag{21}$$

$$u_{\mathrm{R}}^{\mathrm{k=1}} = u - Q_{\mathrm{SHTGV}}^{\mathrm{k=1}} \tag{22}$$

where k denotes the residual iteration number, and $\mathrm{u_R}$ denotes the residual result. Due to the damage of TGV to the effective signals, only one iteration is not the best. It requires multiple iterations to extract the effective information from the residual profile and perform the effective signals stack continuously. Beginning the residual iteration as follow

$$Q_{\mathrm{SHTGV}}^{\mathrm{k+1}} = TGV(SH^{-1}(T(SH(u_{\mathrm{R}}^{\mathrm{k}})))) \tag{23}$$

$$\tilde{u} = \tilde{u} + Q_{\mathrm{SHTGV}}^{\mathrm{k+1}} \tag{24}$$

$$u_{\mathrm{R}}^{k+1} = u_{\mathrm{R}}^{k} - Q_{\mathrm{SHTGV}}^{\mathrm{k+1}} \tag{25}$$

The calculation process is shown in Figure 5. Since random noise contained in the result of each iteration is different, the weight factors α_0 and α_1 in the TGV need to be updated. Given the initial value, the adaptive weights change as the residual profile changes, which are defined as follows

$$\alpha_0 = \alpha_0 \times \frac{u_R^{k+1}}{u_R^k} \alpha_1 = \alpha_1 \times \frac{u_R^{k+1}}{u_R^k} \tag{26}$$

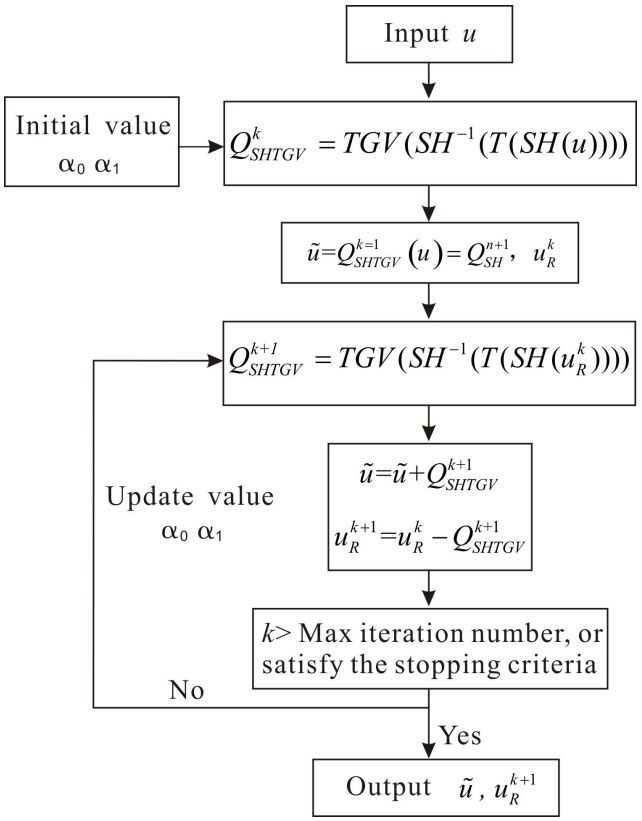

FIGURE 5. Flow chart of iteration for random noise suppression.

Through iterative calculation, the final estimated denoising result $\tilde{u}$ is given until the stopping criterion is met or the maximum number of iterations is reached.

V. SYNTHETIC SEISMIC SIGNALS DE-NOISING TEST

In order to verify the effectiveness of the proposed method, this paper uses the synthetic single-shot seismic signals for verification. As shown in Figure 6 (a), the seismic signals include multiple effective reflected-wave events. The number of the detector is 200. The sampling interval is 0.001s. The number of sampling points is 800. The Gaussian random noise is added into the synthetic seismic signals. The SNR of the seismic signals with random noise is 6.43dB, as shown in Figure 6 (b), which is used to test the denoising ability of the proposed method.

TGV, Wavelet, Curvelet and Shearlet denoising method are used respectively to compare with the proposed method. The denoising results are shown in Figure 7. Figure 7(a) is the Wavelet denoising result. The scale parameter used is 4. In figure 7(a), random noise is suppressed well, but the boundary effect caused by the threshold shrinkage is obvious. Figure 9(a) is the corresponding residual profile. Part of the events can been seen, which indicates effective signals are damaged. Figure 7(b) is the Curvelet denoising result. The scale and angle parameters used are 4 and 16, respectively. In figure 7(b), random noise is suppressed well, and the boundary effect caused by the threshold shrinkage becomes alleviated. That is because Curvelet is sparser than Wavelet.

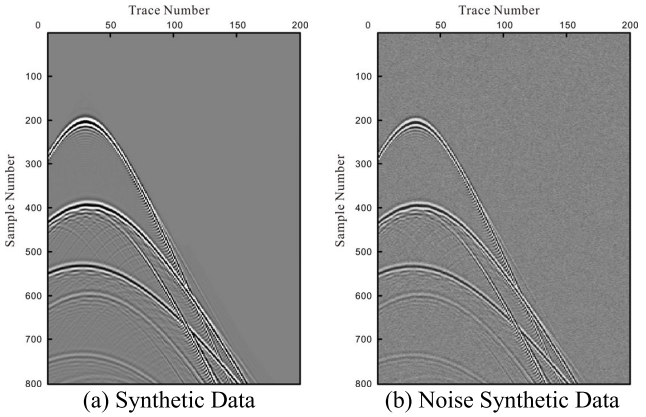

FIGURE 6. Single-shot record of synthetic data.

Figure 9(b) is the corresponding residual profile. It can also see part of effective signals.

Figure 7(c) is the result of the Shearlet denoising method. The scale and angle parameters used are 4 and [1 1 2 2]. Random noise is adequately suppressed and the imaging quality becomes better than the Wavelet and Curvelet denoising results. That is because Shearlet is sparsest. Figure 9 (c) shows the corresponding residual profile. The existence of effective signals is almost invisible. Due to the threshold shrinkage, the boundary effect are produced in Figure 7(c). In order to show the boundary effect better, the local place enclosed by the red dotted line in Figure 7(c) is enlarged, as shown in Figure 8(a). There are obvious 'burrs' on the boundary of the events.

Figure 7(d) is the TGV result. The maximum iteration number is 100. The values of weight factors α_0 and α_1 are 0.1 and 0.15, which are set according to the noise level contained in the signals. Different values of weight factors will affect the number of iterations. Random noise has been suppressed to a certain degree. But the boundary of the reflection events are preserved well. However, the obtained result is not ideal. Due to the interference of random noise, the 'oil painting' effect appears in the result, which influences the seismic imaging quality. Figure 9(d) is the corresponding residual profile. The continuous events can be seen clearly, indicating the effective signals are damaged seriously by TGV.

Figure 7(e) shows the result of the proposed method. The scale and angle parameters used of Shearlet transform are also 4 and [1 1 2 2]. The maximum iteration number of TGV is 100. The initial values of TGV weight factors α_0 and α_1 are 0.03 and 0.05. Compared with TGV, Wavelet, Curvelet and Shearlet methods, the denoising result obtained by the proposed method is better. Random noise is suppressed more thoroughly, and the artificial effects introduced are minimized. The boundary effect and the 'oil painting' effect cannot been seen almost. We enlarge the local place enclosed by the red dotted line in Figure 7(e) as the same as the Shearlet denoising result, as shown in Figure 8(b). The boundary of the events are preserved effectively.

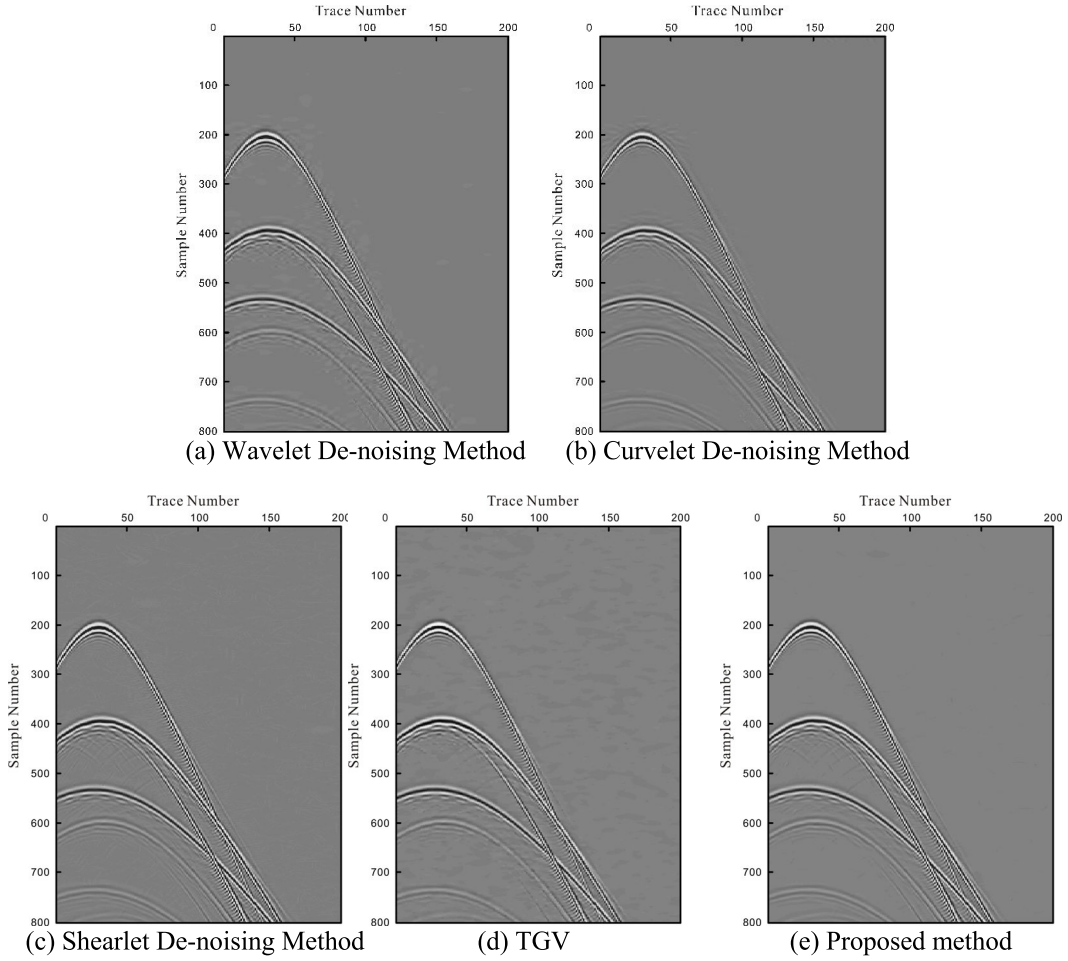

FIGURE 7. De-noising results.

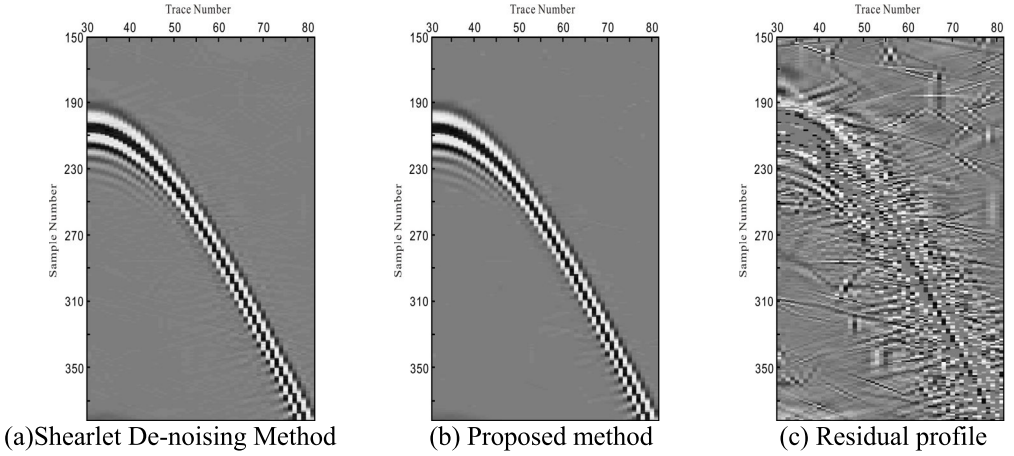

FIGURE 8. Local part comparison of seismic de-noising results.

In order to show the difference between figure 8(a) and 8(b) obviously, the residual profile between them is shown in figure 8(c). It proves the effectiveness of the proposed method.

Here, the denoising process of the proposed method is given. The denoising results and their corresponding residual profiles of $k = 1$, $k = 3$, $k = 5$ and $k = 10$ iterations are shown in Figure 10, respectively. It can obverse that, at the

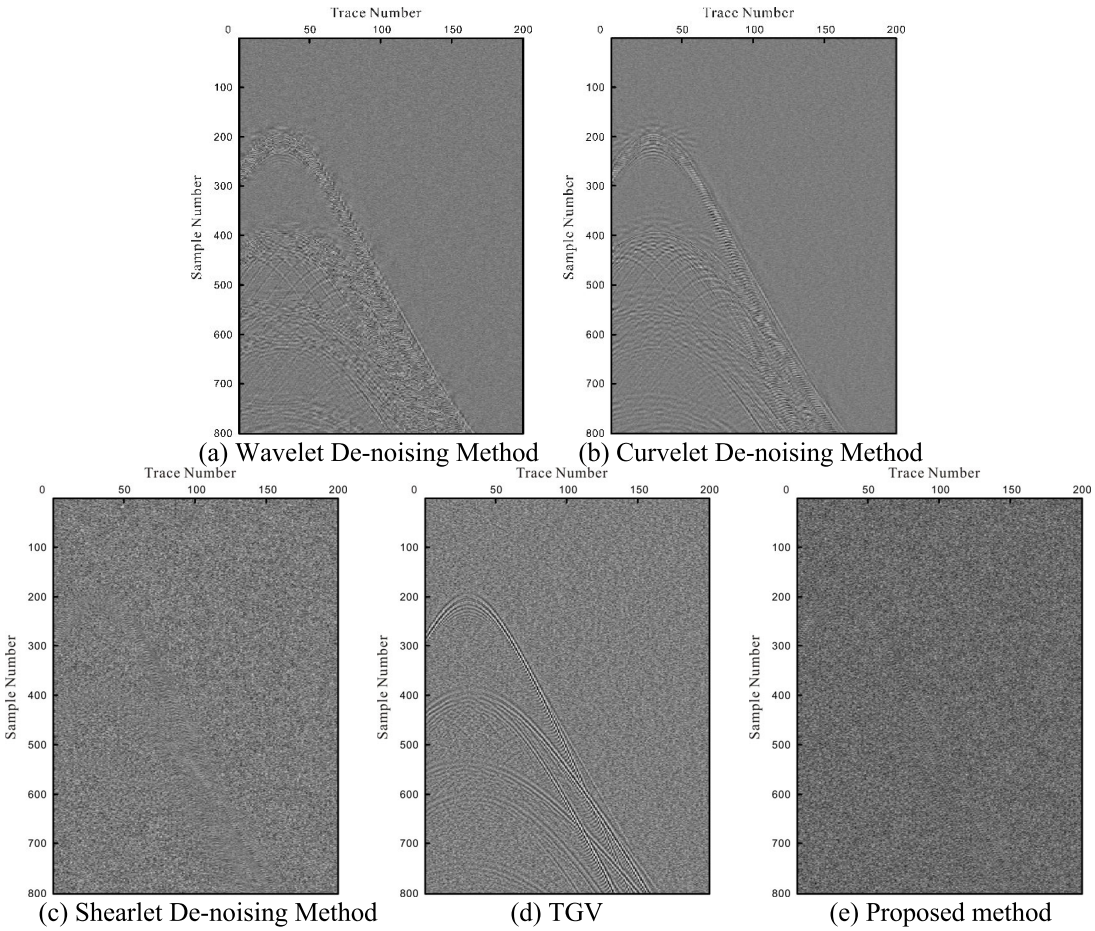

FIGURE 9. Residual profile between noise and de-noising data.

beginning of the iteration, the effective signals contained in the residual profile is relatively obvious. It is necessary to continuously extract the remaining effective signals from the residual profiles and stack until the maximum number of iterations is reached or the mean square error reaches the set minimum value. In this way, the high SNR and fidelity denoising results can be obtained.

In order to quantify the effectiveness of the proposed method, the SNR, peak signal-to-noise ratio (PSNR), mean square error (MSE) and edge-preserving index (EPI) corresponding to different results are calculated in Table 1. It can be seen that in the synthetic data test, compared with other four methods, the proposed method has higher SNR, PSNR and EPI, respectively. At the same time, the MSE of the results obtained by this method is the smallest.

In summary, through the test of the synthetic signals, the proposed method in this paper not only removes random noise, but also suppresses the boundary effect caused by the Shearlet threshold shrinkage and the 'oil painting' effect of TGV, which improves the SNR and fidelity of seismic data. The holistic imaging quality of seismic signals has been improved significantly. The proposed method utilizes the interaction iteration between Shearlet shrinkage threshold and TGV to extract the effective signals from the residual profile. Since the effective signals gradually reduces in the residual profile, the iteration number of TGV will reduce significantly as the input data changes. So the computational complexity of the proposed algorithm won't get very high.

TABLE 1. SNR, PSNR, MSE and EPI of noise seismic data before and after denoising.

	Noise Data	Wavelet	Curvelet	TGV	Shearlet	Proposed
SNR (dB)	6.43	13.35	14.02	9.71	14.64	15.68
PSNR (dB)	58.58	65.42	65.98	61.84	66.65	67.83
MSE	0.091	0.019	0.016	0.043	0.014	0.01
EPI	0.6974	0.9047	0.9402	0.7696	0.9709	0.9896

VI. FIELD SEISMIC SIGNALS DENOISING TEST ONE

Based on the results obtained by the synthetic signals, the method proposed in this paper is applied to field seismic signals. The post-stack profile of the field seismic signals which is used for testing is shown in Figure 11. The post-stack profile contains the fold structures obviously. Random noise influence the identification and judgment of the structure

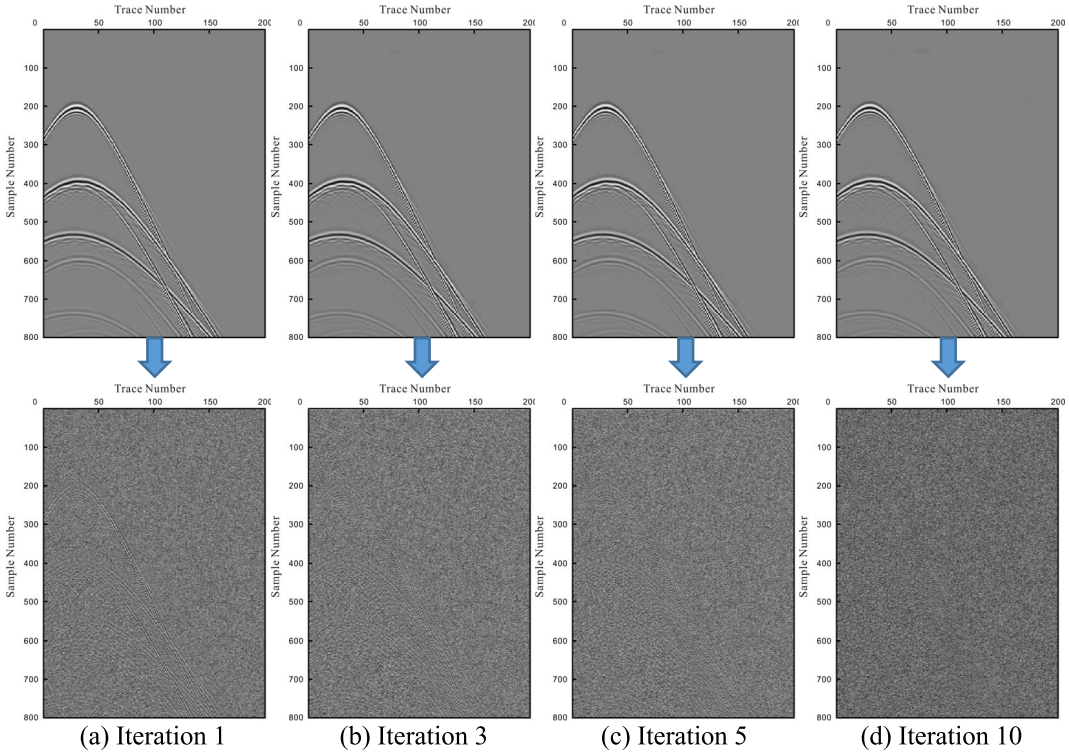

FIGURE 10. Extracted effective-signal results during iteration and corresponding residual profiles.

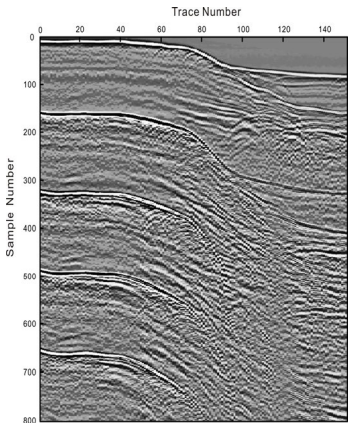

FIGURE 11. Stacking profile of the field seismic data.

boundaries. In Figure 11, some events with strong energy have good continuity. That can be effectively identified. On the other hand, the events with weak energy are drowned by random noise, which is difficult to identify due to the poor continuity. That influences the interpretation and judgment of the geological structures.

TGV, Wavelet, Curvelet, Shearlet denoising method and the proposed method in this paper are used to suppress random noise for the post-stack profile of the field seismic signals. Figure 12(a) shows the Wavelet denoising result. The scale parameter is 4. Figure 13(a) is the corresponding residual profile. There are almost no effective signals. But the de-noising result in figure 12(a) is not ideal. Random noise is not suppressed well. That influences the boundary judgement. Moreover, the boundary effect is shown at the arrow locations obviously due to the threshold shrinkage influence. The red dotted line frame is enlarged in Figure 14(a) in order to better show the boundary effect.

Figure 12(b) is the Curvelet de-noising results with the scale parameter 4 and angle parameter 16. Random noise is suppressed well. That indicates Curvelet transform is sparser than Wavelet transform. But it also cause the boundary effect at the arrow locations due to the threshold shrinkage influence, which is enlarged in figure 14(b). Figure 13(b) is the corresponding residual profile, which almost do not contain effective signals.

Figure 12 (c) is the result of the Shearlet denoising method. The scale and angle parameters are 4 and [1 1 2 2]. Random noise is suppressed well. The effective signals with weak energy are presented, which also have good continuity, especially in the fold structure. All the events can be distinguished and identified effectively. The texture information of the post-stack profile is preserved, and the imaging quality is better. Figure 13(d) is corresponding residual profile. We almost cannot observe the continuous events. That illustrates the Shearlet denoising method has less damage to the effective signals. However, some part of the post-stack profile appear the boundary effect due to the threshold shrinkage in the Shearlet domain. As shown in Figure 14(c), the 'burrs' located at the two arrows of the fold structure between 80 and

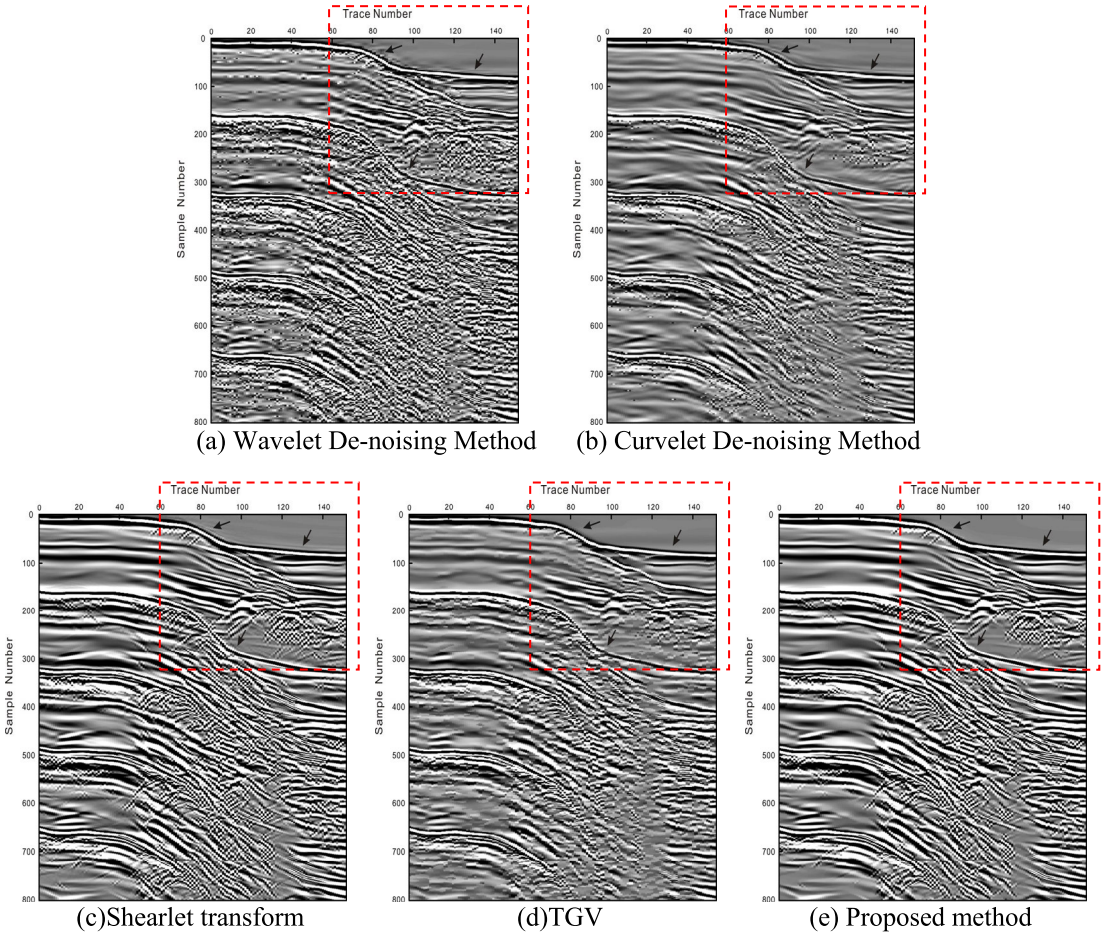

FIGURE 12. De-noising results of the field seismic profiles.

100 is produced due to the bending fold structure. In addition, comparing with the original post-stack profile, it can be seen that a false stratum appears at the arrow in the upper right corner of the post-stack profile.

Figure 12(d) shows the TGV denoising result. The maximum iteration number is 100. The values of weight factors α_0 and α_1 are 10 and 11. Random noise is suppressed, and the events drowned are presented now. However, the strong 'oil painting' effect is produced due to the influence of random noise and the structure complexity. That seriously influences the imaging quality of the post-stack profile, especially the part corresponding to the folds. The poor continuity of the events damages the texture information of the post-stack profile. Figure 13(d) is the residual profile corresponding to the TGV method, which can observe the continuous events. TGV has serious damage to the field seismic profile.

Figure 12(e) is the denoising result of the proposed method. The scale and angle parameters used of Shearlet transform are also 4 and [1 1 2 2]. The maximum iteration number of TGV is 100. The initial values of TGV weight factors α_0 and α_1 are 1 and 3. Comparing with TGV, Wavelet, Curvelet and Shearlet denoising method, it can be seen that the proposed method not only effectively suppresses random noise, but also preserves effective texture information. As shown by the corresponding arrow positions in Figure 14 (e), the 'burrs' and false stratum generated during the calculation process are eliminated. At the same time, the influence of the 'oil painting' effect is subtracted. The SNR and fidelity of the field seismic profile are improved. Figure 13(e) is the corresponding residual profile. The continuous events are hardly observed, indicating that the proposed method has a strong ability to extract effective signals. And the damage to the effective signals is minimal.

VII. FIELD SEISMIC DATA DE-NOISING TEST TWO

Another field seismic signals are used to test the proposed method. The seismic post-stack profile is shown in figure 15, which structure is more complex. Random noise influences the imaging quality of the seismic post-stack profile. The events with weak energy are almost drowned by random noise, which is difficult for the identification and judgment of the structure boundaries.

TGV, Wavelet, Curvelet, Shearlet de-noising method and the proposed method are used to suppress random noise for the post-stack profile. Figure 16(a) is the Wavelet denoising result. The scale parameter is 4. Random noise is suppressed,

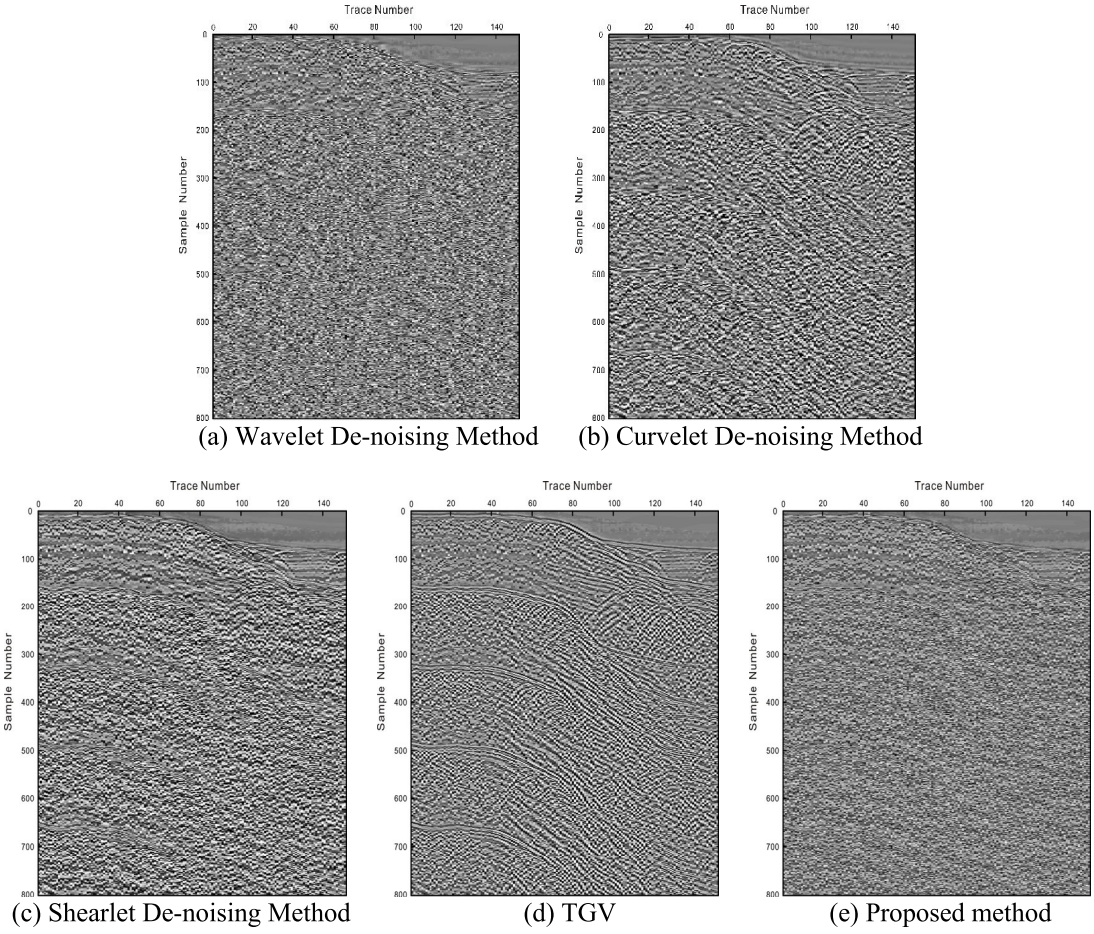

FIGURE 13. Residual profiles of the field seismic de-noising results.

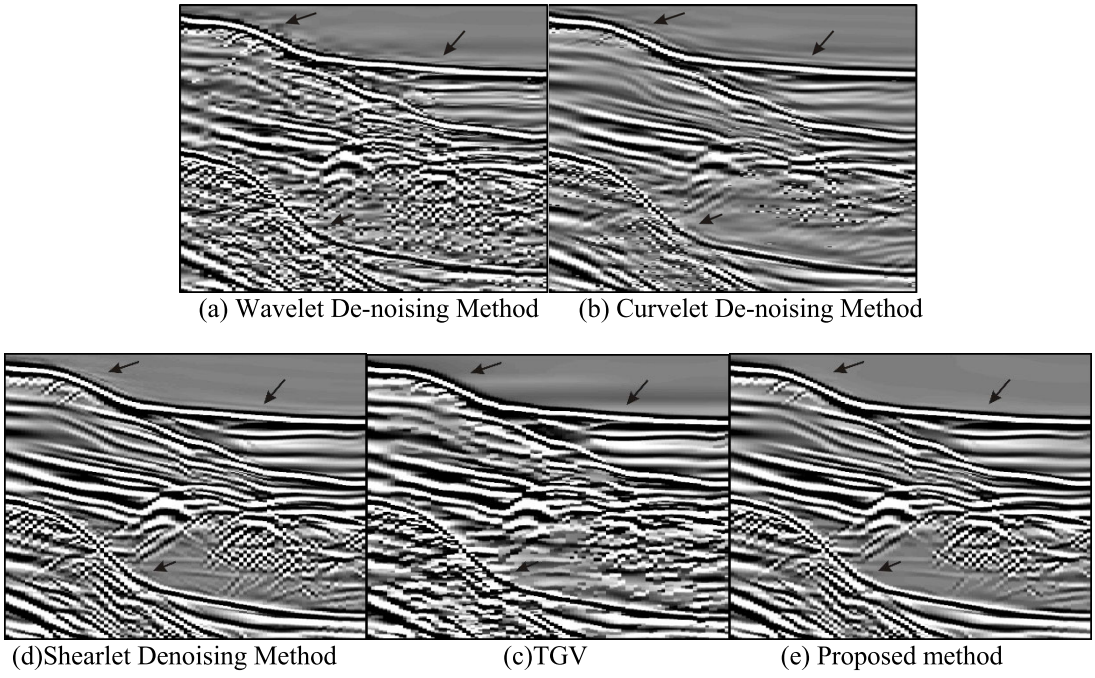

FIGURE 14. Local part comparison of the field seismic de-noising results.

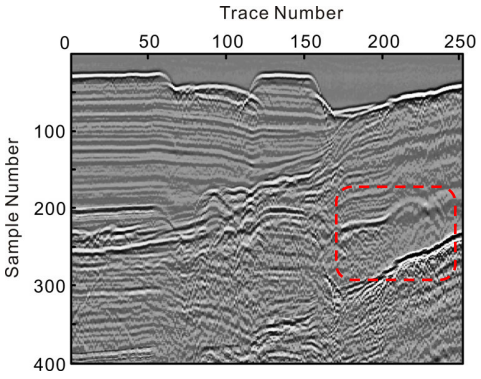

FIGURE 15. Stacking profile of the field seismic data.

but the boundary effect caused is very serious, which reduces the boundary-identification precision, especially at the arrow locations. Figure 17(a) is the corresponding residual profile, which contains less effective signals. Figure 16(b) is the Curvelet denoising result. The scale and angle parameters are 4 and 16. As Curvelet transform is sparser than Wavelet transform, random noise is better suppressed. The boundary effect becomes alleviated. Figure 17(b) is the corresponding residual profile. Figure 16(c) is the Shearlet denoising result. The scale and angle parameters are 4 and [1 1 2 2]. Compare with Wavelet and Curvelet, Shearlet transform is sparser, so the de-noising result obtained is best. The boundary effect becomes alleviated further.

Figure 16(d) is the TGV result. The maximum iteration number is 100. The values of weight factors α_0 and α_1 are 10 and 11. Random noise is suppressed well. But the 'oil painting' effect appears in the result. And the 'oil painting'

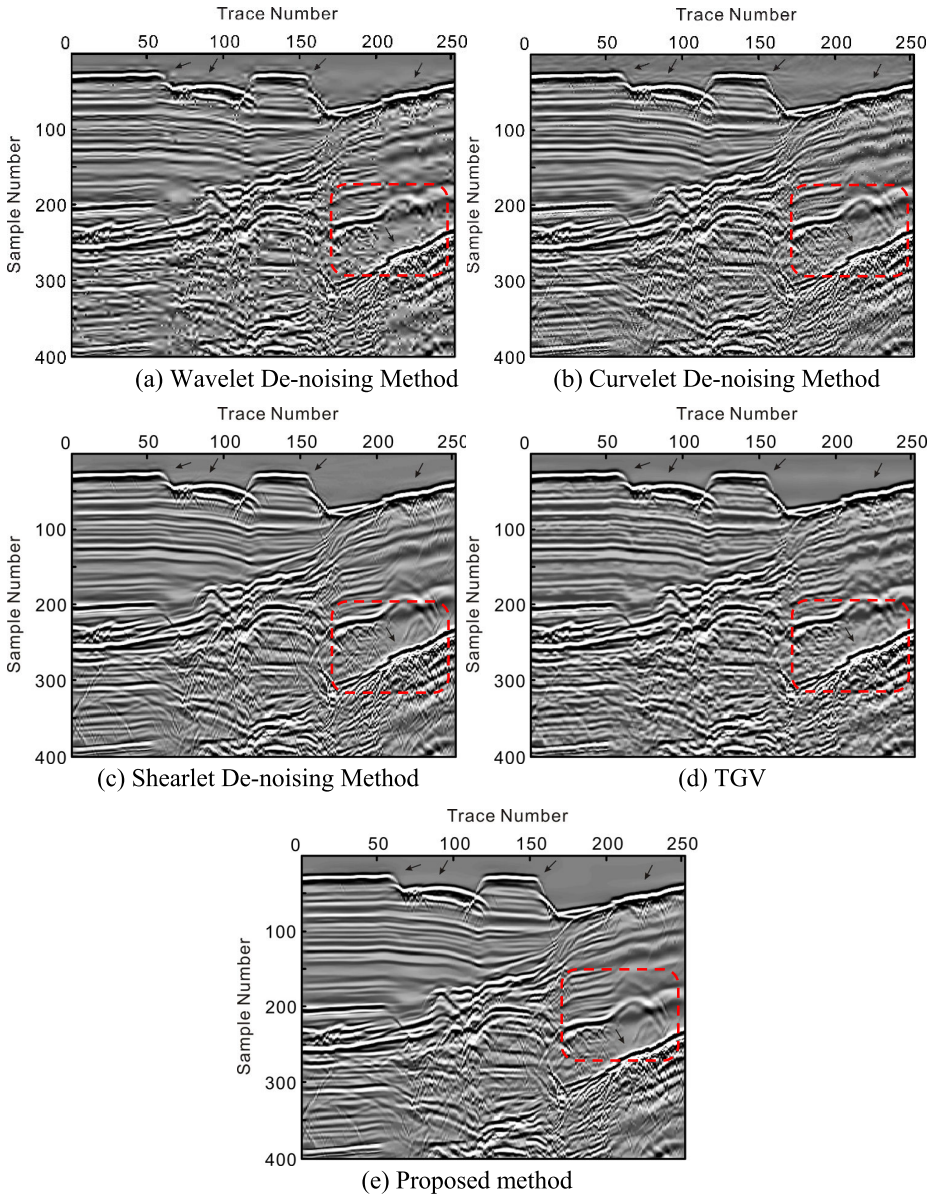

FIGURE 16. De-noising results of the field seismic profiles.

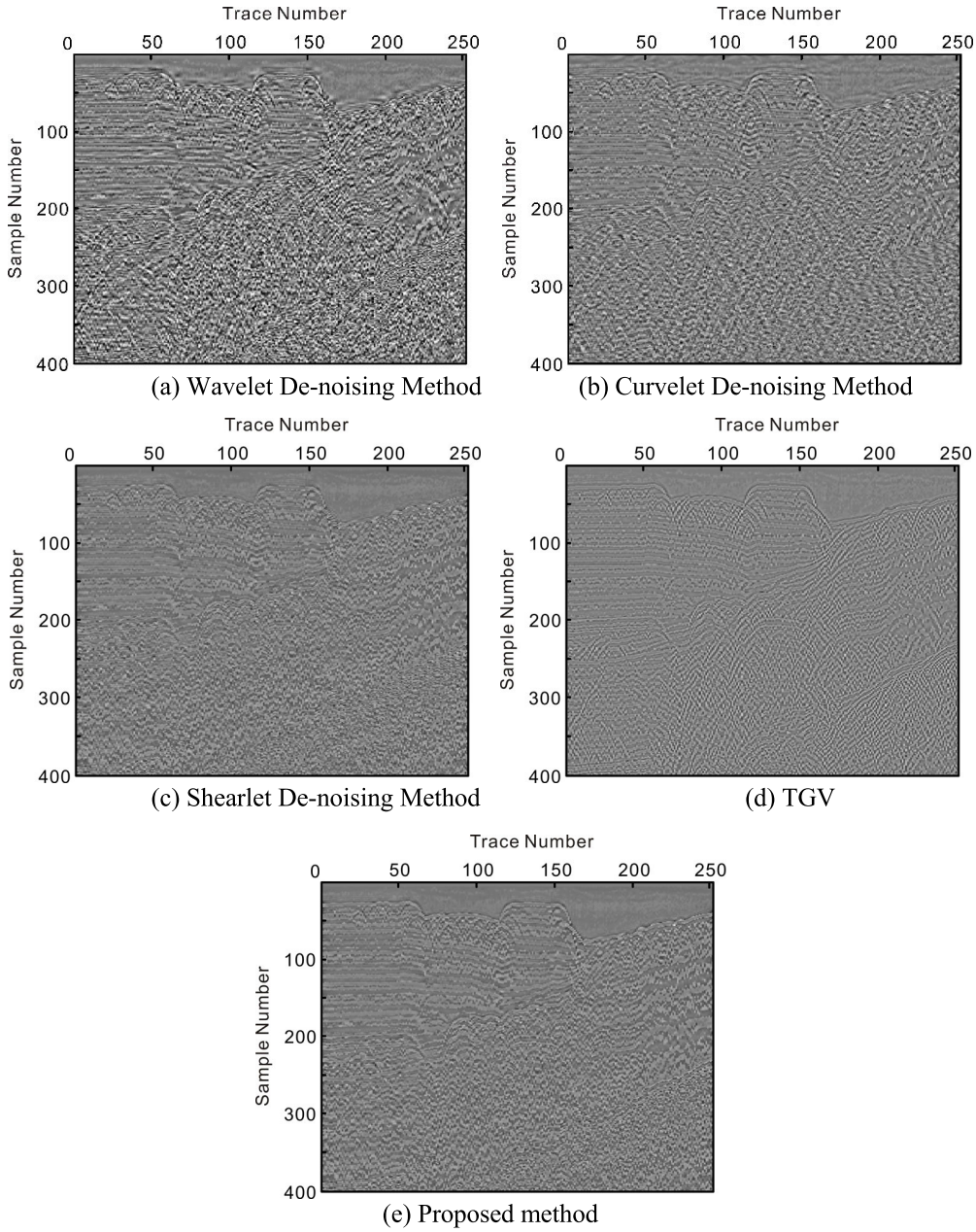

FIGURE 17. Residual profiles of the field seismic de-noising results.

effect becomes more serious at where the structure is complex. Figure 17(d) is the corresponding residual profile, which the event shape of the effective signals is obvious.

Figure 16(e) is the de-noising result obtained by the proposed method. The scale and angle parameters used of Shearlet transform are also 4 and [1 1 2 2]. The maximum iteration number of TGV is 100. The initial values of TGV weight factors α_0 and α_1 are 1 and 3. Random noise is suppressed effectively. And the texture information is preserved. As shown by the corresponding arrow positions in Figure 16 (e), the boundary effect generated during the calculation process are eliminated. At the same time, the influence of the 'oil painting' effect is subtracted. Figure 17(e) is the corresponding residual profile.

VIII. CONCLUSION

This paper proposes a joint framework for seismic signal de-noising using Shearlet threshold shrinkage and TGV, which makes full use of their characteristics. Through the interactive iteration between Shearlet threshold shrinkage and TGV, the best estimated denoising result can be obtained. Comparing with wavelet, Curvelet, Shearlet and TGV de-noising methods through the synthetic and field seismic data, it proves that the proposed method not only

can suppress random noise, but also preserve the boundary and texture information effectively. And it improves the SNR and fidelity of the seismic data significantly. Through the research, we can find that one specific denoising method is not possible, as all de-noising methods have their individual benefits and drawbacks. The joint denoising method is our future development direction.

REFERENCES

[1] H. Zhu, Z. Zeng, H. Zeng, and C. Xu, "3D seismic data attribute-based characterization of volcanic reservoirs in the BZ34-9 block, bohai bay basin, eastern China," *Geophysics*, vol. 85, no. 3, pp. IM1–IM13, May 2020.

[2] Y. Ma, C. Yuan, and J. Zhang, "Joint microseismic event location and anisotropic velocity inversion with the cross double-difference method using downhole microseismic data," *Geophysics*, vol. 85, no. 3, pp. KS63–KS73, May 2020.

[3] F. Poletto, F. Miranda, B. Farina, and A. Schleifer, "Seismic-while-drilling drill-bit source by ground force: Concept and application," *Geophysics*, vol. 85, no. 3, pp. MR167–MR178, May 2020.

[4] X. Zhang, X. Feng, Z. Zhang, Z. Kang, Y. Chai, Q. You, and L. Ding, "Dip filter and random noise suppression for GPR B-Scan data based on a hybrid method in f-x domain," *Remote Sens.*, vol. 11, no. 18, p. 2180, Sep. 2019.

[5] X. Kong, Y. Zhao, J. Xue, and J. C.-W. Chan, "Hyperspectral image denoising using global weighted tensor norm minimum and nonlocal low-rank approximation," *Remote Sens.*, vol. 11, no. 19, p. 2281, Sep. 2019.

[6] T. Pan, D. Peng, W. Yang, and H.-C. Li, "A filter for SAR image despeckling using pre-trained convolutional neural network model," *Remote Sens.*, vol. 11, no. 20, p. 2379, Oct. 2019.

[7] H. Lin, H. Ma, Y. Li, and D. Shao, "Elimination of seismic random noise based on the SW statistic adaptive TFPF," *Chinses J. Geophys.*, vol. 58, no. 12, pp. 4559–4567, Dec. 2015.

[8] S. Liu, Q. Hu, P. Li, J. Zhao, M. Liu, and Z. Zhu, "Speckle suppression based on weighted nuclear norm minimization and grey theory," *IEEE Trans. Geosci. Remote Sens.*, vol. 57, no. 5, pp. 2700–2708, May 2019.

[9] Z. Yan, X. Luan, Y. Wang, J. Pan, G. Fang. ;., and J. Shi, "Seismic random noise attenuation based on empirical mode decomposition of fractal dimension," *Chinses J. Geophys.*, vol. 60, no. 7, pp. 2845–2857, Jul. 2017.

[10] C. Wang, Z. Zhu, H. Gu, X. Wu, and S. Liu, "Hankel low-rank approximation for seismic noise attenuation," *IEEE Trans. Geosci. Remote Sens.*, vol. 57, no. 1, pp. 561–573, Jan. 2019.

[11] J. Wang, Q. Li, X. Xu, and L. Cao, "Random noise attenuation method of seismic signal based on the fractional order wavelet domain GSM model," *Chin. J. Geophys.*, vol. 61, no. 7, pp. 2989–2997, Jul. 2018.

[12] X. Zhao, Y. Li, G. Zhuang, C. Zhang, and X. Han, "2-D TFPF based on contourlet transform for seismic random noise attenuation," *J. Appl. Geophys.*, vol. 129, pp. 158–166, Jun. 2016.

[13] D.-L. Wang, Z.-F. Tong, C. Tang, and H. Zhu, "An iterative curvelet thresholding algorithm for seismic random noise attenuation," *Appl. Geophys.*, vol. 7, no. 4, pp. 315–324, Dec. 2010.

[14] K. Guo, D. Labate, W.-Q. Lim, G. Weiss, and E. Wilson, "Wavelets with composite dilations," *Electron. Res. Announcements Amer. Math. Soc.*, vol. 10, no. 9, pp. 78–87, Aug. 2004.

[15] K. Guo, D. Labate, W.-Q. Lim, G. Weiss, and E. Wilson, "Wavelets with composite dilations and their MRA properties," *Appl. Comput. Harmon. Anal.*, vol. 20, no. 2, pp. 202–236, Mar. 2006.

[16] K. Guo and D. Labate, "Optimally sparse multidimensional representation using shearlets," *SIAM J. Math. Anal.*, vol. 39, no. 1, pp. 298–318, Jan. 2007.

[17] S. Liu, M. Liu, P. Li, J. Zhao, Z. Zhu, and X. Wang, "SAR image denoising via sparse representation in shearlet domain based on continuous cycle spinning," *IEEE Trans. Geosci. Remote Sens.*, vol. 55, no. 5, pp. 2985–2992, May 2017.

[18] S. Q. Liu, S. H. Hu, Y. Xiao, and Y. L. An, "Bayesian shearlet shrinkage for SAR image de-noising via sparse representation," *Multidimensional Syst. Signal Process.*, vol. 25, no. 4, pp. 683–701, Oct. 2014.

[19] C. Liu, D. Wang, T. Wang, F. Feng, H. Cheng, and G. Meng, "Random seismic noise attenuation based on the Shearlet transform," *Acta Petrolei Sinica*, vol. 35, no. 4, pp. 692–699, Jul. 2014.

[20] H. Cheng, G. Chen, E. Wang, Z. Hou, and J. Fu, "Seismic data de-noising method of adaptive threshold based on Shearlet transform," *Acta Petrolei Sinica*, vol. 39, no. 1, pp. 82–91, Jan. 2018.

[21] H. Cheng, D. Wang, E. Wang, J. Fu, and Z. Hou, "Seismic random noise suppression based on scale-adaptive 3D-Shearlet transform," *Oil Geophys. Prospecting*, vol. 54, no. 5, pp. 970–978, Oct. 2019.

[22] L. I. Rudin, S. Osher, and E. Fatemi, "Nonlinear total variation based noise removal algorithms," *Phys. D, Nonlinear Phenomena*, vol. 60, nos. 1–4, pp. 259–268, Nov. 1992.

[23] K. Bredies, K. Kunisch, and T. Pock, "Total generalized variation," *SIAM J. Imag. Sci.*, vol. 3, no. 3, pp. 492–526, 2010.

[24] S. Durand and J. Froment, "Reconstruction of wavelet coefficients using total variation minimization," *SIAM J. Sci. Comput.*, vol. 24, no. 5, pp. 1754–1767, Jan. 2003.

[25] H. Hu, H. Sun, C. Deng, X. Chen, and Z. Liu, "Shearlet shrinkage denoising based on total variation regularization," *J. Image Graph.*, vol. 16, no. 2, pp. 168–173, Feb. 2011.

[26] G. Tang and J. Ma, "Application of total-variation-based curvelet shrinkage for three-dimensional seismic data denoising," *IEEE Geosci. Remote Sens. Lett.*, vol. 8, no. 1, pp. 103–107, Jan. 2011.

[27] D. Kong and Z. Peng, "Seismic random noise attenuation using shearlet and total generalized variation," *J. Geophys. Eng.*, vol. 12, no. 6, pp. 1024–1035, Dec. 2015.

XIANNAN WANG received the Ph.D. (Eng.) degree in geophysical prospecting and information technology from Jilin University, China, in 2018. Her research interest includes signal processing with applications to seismic wave data. Since 2019, she has been engaged in seismic wave research with the School of Equipment Engineering, Shenyang University of Science and Technology.

JIAN ZHANG was born in 1961. He received the master's and Ph.D. degrees from Northeastern University, China.

He is currently a Professor and a Doctoral Supervisor. He is also the Vice President of the Shenyang University of Science and Technology. His main research directions include target detection and identification technology. He has presided over the completion of more than ten national scientific research projects and published more than 40 academic articles. Many of his achievements won the National Science and Technology Award and the Liaoning Province Teaching Achievement Award.

HAO CHENG was born in Shenyang, China, in 1988. He received the Ph.D. degree in geophysical prospecting and information technology from Jilin University, Changchun, China, in 2016.

He held a postdoctoral position in geophysical prospecting and information technology with Northeastern University, Shenyang, in 2019, where he has been a Lecturer with the School of Resources and Civil Engineering, since 2019. His research interests include the wave-field reconstruction of passive seismic data, seismic random noise attenuation, and compressed sensing.